WiDir: Walking Direction Estimation Using Wireless Signals

Dan Wu[1,2], **Daqing Zhang**[1,2], **Chenren Xu**[3,2], **Yasha Wang**[4,2], **Hao Wang**[1,2]

[1]Key Laboratory of High Confidence Software Technologies, Ministry of Education, Beijing, China
[2]School of Electronics Engineering and Computer Science, Peking University, China
[3]Center for Energy-efficient Computing and Applications, Peking University, China
[4]National Engineering Research Center of Software Engineering, Peking University, China
{dan, dqzsei, chenren, wangyasha, haowangsei}@pku.edu.cn

ABSTRACT

Despite its importance, walking direction is still a key context lacking a cost-effective and continuous solution that people can access in indoor environments. Recently, device-free sensing has attracted great attention because these techniques do not require the user to carry any device and hence could enable many applications in smart homes and offices. In this paper, we present WiDir, the first system that leverages WiFi wireless signals to estimate a human's walking direction, in a device-free manner. Human motion changes the multipath distribution and thus WiFi Channel State Information at the receiver end. WiDir analyzes the phase change dynamics from multiple WiFi subcarriers based on Fresnel zone model and infers the walking direction. We implement a proof-of-concept prototype using commercial WiFi devices and evaluate it in both home and office environments. Experimental results show that WiDir can estimate human walking direction with a median error of less than 10 degrees.

ACM Classification Keywords

C.3 Special-Purpose and Application-Based Systems: Miscellaneous

Author Keywords

Channel State Information (CSI); WiFi; Fresnel Zone; Direction Estimation

INTRODUCTION

Many emerging applications in smart home and elderly care are predicated on the belief that knowing one's real-time context can greatly improve people's safety, efficiency and quality of life. There have been many ways and techniques proposed for context sensing, ranging from wearable sensor-based, ambient device-based to computer vision based solutions. Wearable sensor-based approaches were among the most popular techniques developed for location and direction sensing [10]. These systems can only work when sensors are worn by the user. However, the always-on-body requirement makes the subject difficult to comply with, especially for the elders at home. Ambient device-based approaches try to make use of ambient information to sense context. The ambient information being used includes audio[31], floor vibration[5] and infrared sensing data[3]. In these systems, dedicated devices need to be implanted in the environment. Computer vision-based approaches use cameras installed in the environment to either capture images or video sequences for context recognition. Although the recent advances in infra-red LED and depth camera like Microsoft Kinect [32], have enlarged its application scope (e.g., independent of illumination of lights and can work even in a dark room), the privacy intrusion, inherent requirement for line of sight and intensive computation for real-time processing are still open issues that need to be addressed in the future [17].

In recent years, the rapid development in wireless techniques has stimulated the research in studying the relationship between the wireless signal and context sensing. In particular, the recently exposed physical layer Channel State Information (CSI) on commercial WiFi devices reveals multipath channel features at the granularity of OFDM subcarriers [4], which is much finer-grained than the traditional MAC layer RSS (Received Signal Strength). By exploiting the amplitude and phase information of CSI across the OFDM subcarriers and the diversity of CSI information across multi-antennas in MIMO systems, significant progress has been made in applications in localization [42, 40, 15], motion detection [14, 25], lip language [33], gesture recognition [24, 22], vital sign monitoring [20, 19], breathe estimation [11, 23, 27], fall detection [6, 48, 34] and activity recognition [37]. The rationale behind all these research efforts is that different human activities can affect the electromagnetic field of wireless signals and cause different signal change patterns, and activities can be recognized in real-time by mapping the observed signal change patterns to different human activities.

Despite its importance, walking direction is still a key context lacking a cost-effective and continuous solution that people can access in indoor environments. With one's location and moving direction, indoor applications such as emergency evacuation, virtual reality and activity tracking of elders can be enabled and enhanced, where each individual's movement di-

UbiComp '16, September 12-16, 2016, Heidelberg, Germany
 ISBN 978-1-4503-4461-6/16/09…$15.00
DOI: http://dx.doi.org/10.1145/2971648.2971658

rection and trajectory needs to be tracked accurately. In the context of assisted living, a single user's location and moving direction is important for a number of services ranging from monitoring daily activities, forecasting user tendencies, to smart control of appliances [29]. Monitoring moving direction in real-time also helps to improve performance of localization [35] and tracking applications when combined with distance or speed information. WalkCompass [28] is an example showing how walking direction can improve the localization results on a smartphone.

While both device-based and device-free location sensing techniques using COTS WiFi devices have been actively explored [46, 40, 1, 42, 15], the state-of-the-art device-based and device-free approach achieves submeter-level[15] and meter-level[1] accuracy, respectively. Both are too coarse to derive accurate moving direction directly.

In this paper, we present WiDir, a CSI-based device-free human walking direction detection system. To our best knowledge, WiDir is the first system that can estimate moving direction using WiFi CSI information in device-free manner. First, we introduce the Fresnel zone model in the indoor environment and develop the model in the context of multi-path propagation in theory, and then relate the reflection-induced phase change at the receiver end to the location in Fresnel zone. Then by integrating the phase analysis from multiple subcarrier waveforms into Fresnel zone, we are able to estimate 1) if the walking direction is inwards or outwards the Fresnel zone, which we call Fresnel direction, and 2) the walking distance in this direction. Finally, we propose a temporal-spatial model to estimate the walking direction.

Mapping this high-level idea into a practical system, however, poses several challenges. First, how to derive direction information using the CSI information from all the available subcarriers. Further more, a walking human behaves very differently from a moving smooth metal object, leading to very noisy signals at the receiver device. Our solution lies in the fact that phase difference between two subcarriers leads to delay in time. By measuring cross-correlation between two subcarriers, we are able to extract Fresnel direction information from it.

A second challenge stems from the fact that with a single Fresnel zone, we can neither detect the direction from all angles, nor derive the walking direction in the local Cartesian coordinate system. We tackle this problem by strategically placing multiple WiFi devices to form interleaved Fresnel zones and combining the derived motion direction and distance information to address the issues mentioned above.

Unlike Walkcompass a user carries can't estimate the walking direction accurately until the user walks a few steps, WiDir offers consistent direction estimation performance, which is comparable with WalkCompass. The experiment shows WiDir achieves a mean absolute error of 10.54 degrees and median absolute error of 8.62 degrees in empty rooms. In normal office rooms WiDir obtains a mean absolute error of 15.51 degrees and median absolute error of 11.49 degrees. WiDir is capable to run in real-time and continuously estimate the walking direction for paths like circle and zigzag.

This paper makes the following contributions:

- We define and propose how to estimate Fresnel direction with the insight that the phase information in two different subcarriers conveys the delay information, based on our developed Fresnel zone model and multi-frequency phase analysis.
- We propose a 2D Fresnel zone model and validate that it can be used to effectively estimate the Fresnel direction and distance in a local Cartesian coordinate system and further derive the walking direction.
- We implement WiDir system using commercial WiFi devices and evaluate in rooms of different shape and size. Our experiments show that WiDir can estimate walking direction angle in real time, robust to environmental change, with the median error of less than 10 degrees.

BACKGROUND

In this section, we overview the relevant background knowledge and introduce the key take-away messages for our work.

Phase Change of Radio Wave Propagation and Reflection

In indoor radio propagation, the receiver often receives the signals not only from the direct path (Line-of-Sight, LoS), but also massive multi-path (Non-Line-of-Sight, NLoS) components caused by reflection, diffraction and scattering. All three of these phenomenon cause signal distortion and fading [26]. When multiple paths co-exist, the received signal can be expressed as a summation of all the paths, which we call wave *superposition*. For radio wave of wavelength λ, when it travels along a path of length d, its phase shifts $2\pi d/\lambda$. This can be expressed as vector sum $\sum a_i e^{-j2\pi d_i/\lambda}$ where i is path number and a means attenuation coefficient of each path. If the environment is static and none of these paths change in length, the final vector remains static.

Fresnel Zone

Fresnel zone [26] is a series of concentric ellipsoidal regions of alternating reinforced strength and weakened strength of a wave's propagation, caused by a wave following multiple paths as it passes by an object and is partially diffracted/reflected by it, resulting in constructive and destructive interference as the different length paths go in and out of phase, as shown in Figure 1. That being said, when reflective surfaces (e.g., human body) is along a radio propagation path, the radio waves reflecting off those surfaces may arrive either out of phase or in phase with the signals that travel directly to the receiver, depending on the reflector's relative location to the pair of transmitter and receiver.

WiFi CSI

Channel Status Information (CSI) is information that estimates the channel by representing the channel properties of a communication link [40]. Channel state $H(f,t)$ for carrier frequency f is described by channel frequency response (CFR). It has the relation $Y(f,t) = H(f,t)X(f,t)$, where $X(f,t)$ and $Y(f,t)$ are signals of transmitted and received in frequency domain. In WiFi 802.11n, CSI is measured and reported at the scale of OFDM subcarriers. The number of subcarriers in 802.11n

depend on bandwidth configurations. A 20 MHz channel have 56 OFDM subcarriers (index from -28 to -1 and 1 to 28)with a carrier separation of 0.3125 MHz. The total occupied bandwidth is 17.8 MHz. Frequency of each subcarrier can be expressed as $f_{carrier} + 0.3125k$, where $f_{carrier}$ is frequency of central carrier wave and k is subcarrier index. CSI is reported as a single value for Ng adjacent subcarriers. Number of group (Ng) is allowed as 1, 2 and 4 in 802.11n-2009 specs [8], and the choice of Ng is leaved to manufacturers. For example, implementation of Intel 5300 wireless NIC report total 30 CSI values for both 20MHz ($Ng = 2$) and 40MHz ($Ng = 4$) configurations. This means each CSI subcarrier are spaced in 2×0.3125MHz (expect subcarrier indexes -2,-1 and 27,28) and 4×0.3125MHz, respectively. A 40MHz channel can have as many as 114 OFDM subcarriers. Each subcarriers are also spaced in 0.3125MHz.

What We Learned for This Work

Let us consider a scenario that there is one pair of TX-RX and one reflector in the target space, as shown in Figure 2. We assume there are two paths between them, namely, d_0 for the direct path and d_1 for the reflected path. In a real environment, d_0 is direct path plus all the other multi-path except for d_1 introduced by the moving reflector. Putting together, we learn the following things to be useful for our work:

- As long as a reflector is moving on the ellipse, it causes the constant effect on the wave superposition, regardless of its location. Let TX and RX be the foci of the ellipse, the distance traveled from one focus to another, via some point on the ellipse, is the same regardless of the point selected.

- When a reflector moves off the ellipse, signals from d_0 and d_1 interfere with each other in a predictive way - most constructively when phase change of d_1 and d_0 differs in $k\lambda$, or on the opposite way when phase change of d_1 and d_0 differs in $k\lambda + \lambda/2$; when d_1 changes $k\lambda$, the phase remains unchanged, as shown in Figure 2.

FRESNEL DIRECTION

In this section, we first analyze the Fresnel zone model to study how the signal strength changes at the receiver end when a reflector appears in different locations in the context of Fresnel zone. Then we present how to estimate if the walking direction is inwards or outwards the Fresnel zone (in-zone direction) based on multi-frequency phase analysis. We define this in-zone direction as the Fresnel direction to form the basis for walking direction estimation in a local Cartesian coordinate.

Phase Analysis in Fresnel Zone

As briefly reviewed in Section 2, in a scenario that Tx and Rx are fixed, as long as the reflector doesn't block the direct path, a reflector will create a reflected path which superimposes the wave in the direct path, result in constructive or destructive interferences depending on whether the two paths go in or out of phase. Fresnel zone illustrates the relationship of reflector's location and its impact on the instantaneous CFR power - it comprehensively marks positions in which power is enhanced or degraded. We define *Fresnel phase* ρ as phase difference of signals from the direct path d_0 and the reflected path d_1:

$$\rho = 2\pi(d_1 - d_0)/\lambda + \varphi, \tag{1}$$

in which λ is wavelength of signal, and φ is the extra phase introduced by diffraction/reflection. This extra phase is decided by electric polarization according to plane of incidence and relative permittivity between air and obstacles [7]. All the points a reflector have for the same Fresnel phase ρ create a *Fresnel Equiphase Contour*. We can always find peak signal strength at $\rho = 2k\pi$ and valleys at $\rho = (2k+1)\pi$. Let the instantaneous CFR power of the direct path be a and that of the reflected path be b, let ρ be Fresnel phase, the resulting instantaneous CFR power c at Rx is given by law of cosine:

$$c^2 = a^2 + b^2 + 2ab\cos\rho \tag{2}$$

which means the instantaneous CFR power in time series gives sinusoid-like fluctuation when the length of the reflected path continuously changes as the reflector moves, which is also observed in [36]. To this end, we know that when a reflector moves and changes its reflected path, the instantaneous CFR power will go up and down as it adds in or out phase effect alternatively. That is to say, if we observe such fluctuation, we know the reflector is continuously moving cross the equiphase contours of the Fresnel zone, but we don't know the direction yet - inwards or outwards the Fresnel zone.

Multi-frequency Phase Analysis

Based on the discussion above, we understand the limitation of using Fresnel zone of a single subcarrier in moving direction estimation. If we have multiple (at least two) concentric Fresnel zones with similar shape but slightly different size, we can imagine that as the reflector moves, it will go across one and the other in sequence, and it's easy to infer if the walking direction is inwards or outwards the Fresnel zone. Specifically, we define *Fresnel direction* as positive for outwards the Fresnel zone, and negative in the opposite direction. We note that each subcarrier will create their own Fresnel zone independently of similar shape but different size. Thus, we propose to introduce the multi-frequency Fresnel zone model and we believe it is feasible because: First, for WiFi 802.11n we already use everywhere today, any given channel already provides multiple subcarriers with separate frequencies.That being said, there is zero extra experimental setup overhead to obtain such information from multiple channels. Second, assume there are two subcarriers of wavelength $\lambda_1 < \lambda_2$, from Equation 1, we observe that when two subcarriers have the same Fresnel phase ρ, the subcarrier with shorter wavelength has shorter reflected-path length, thus smaller ellipsoids. In other words, a positive Fresnel direction means for the two Fresnel zones which have the same ρ, the reflector goes across the eclipse of λ_1 first.

To generalize our statement, when the length of the reflected path d_1 is fixed, for all the WiFi subcarriers, the one with a shorter wavelength has a larger ρ. In Figure 3 , for two subcarriers of wavelength $\lambda_1 > \lambda_2$, as people walking inwards Fresnel zones, the length of reflected path d_1 gets shorter and Fresnel phase ρ rotates clockwise. The waveforms of two subcarriers have time delay Δt caused by difference of each

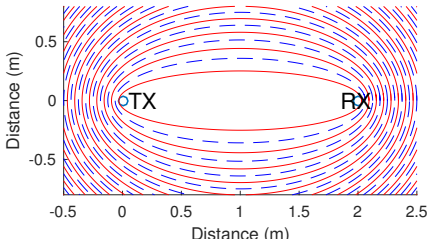

Figure 1. Fresnel Zones around Tx/Rx in 2.4G WiFi. Ellipses in solid and dashed lines indicate the most reinforced and degraded locations of reflector.

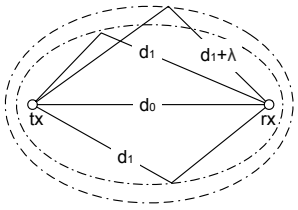

Figure 2. The three reflected paths have the same phase.

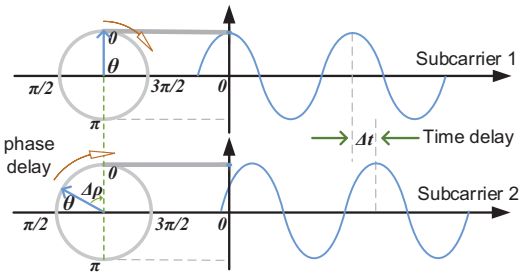

Figure 3. Delay in phase and delay in time of two subcarriers (wavelength in subcarrier 2 is shorter) while people walk inwards Fresnel zones.

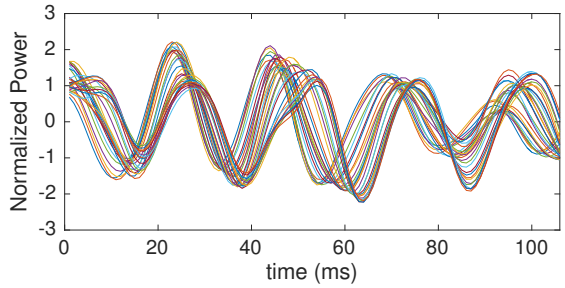

(a) Delayed waveforms for all 30 subcarriers

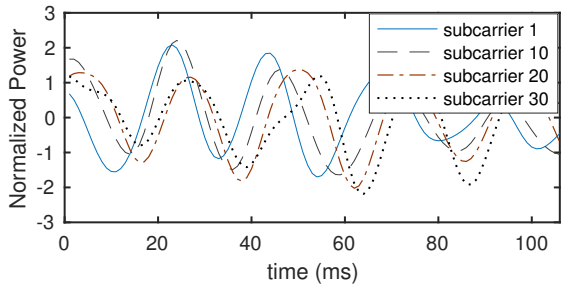

(b) Delayed waveforms for subcarrier 1,10,20 and 30

Figure 4. Delayed waveforms of CSI subcarriers in a walk. the two picture is the same except (b) select 4 subcarriers out of 30 (a). we see precedence relationship between subcarriers. All the waveforms have been Z normalized and denoised before comparing.

initial Fresnel phase ρ. Therefore, when a reflector is moving and has a negative Fresnel direction, we will observe that the sinusoid-like instantaneous CFR power waveform in all subcarriers fluctuates with precedence relationship. The fluctuation occurs first in the subcarrier with longer wavelength (lower frequency), then the shorter one, as shown in Figure 4. By measuring the phase difference of two waveforms from different subcarriers, we are able to obtain the Fresnel direction. Because the Fresnel zone of different subcarriers are concentric, mathematically, for any two subcarriers of wavelength λ_1 and λ_2, we have the phase difference:

$$\Delta\rho = 2\pi(d_1 - d_0)(\frac{1}{\lambda_1} - \frac{1}{\lambda_2}) = 2\pi(d_1 - d_0)(f_1 - f_2)/c \quad (3)$$

that is:

$$\Delta\rho = 2\pi(d_1 - d_0)\Delta f/c, \quad (4)$$

where f_1 and f_2 are frequencies of two subcarriers and c is light speed in air.

It is important to note that from Equation 4, the undermined extra phase φ is canceled out. Thus, the phase difference Δρ is only related to reflected path length d_1 and frequency difference Δf of two subcarriers. This has two implications: First, once the two subcarriers are chosen, a longer reflected path will lead to a larger phase difference Δρ. Second, Δρ is only relevant to the difference of two frequencies, not the carrier frequency itself. Therefore, once the reflector's position is fixed, the larger frequency difference two subcarriers have, the larger phase difference Δρ we have. This information gives us the flexibility to choose the best pair of subcarriers for our use.

However, as the reflected path length d_1 increases, the Δρ will reach π, at which the valleys in one subcarrier's waveform will align with the peaks in another's. At this moment, we are not able to tell which one comes first, as shown in Figure 5(d). In other words, even though we can observe the phase delay between two subcarriers' waveforms, we are not able to tell who comes first, so as to the Fresnel direction. Therefore, we need to choose an optimal phase difference range to guide our choice of the subcarriers - a small difference will make two waveforms too close to be differentiable, and a big difference will lead to the ambiguity we show in Figure 5. Remind that multi-paths cause distortion and random phase shift to the waveform. Therefore, we empirically choose $\pi/2$ as the maximum allowable phase delay to guide our choice of subcarriers. Based on Equation 4, we find that once the phase delay Δρ is fixed, we need to tweak Δf based on d_0 and d_1, i.e., the size of target area. For example, according to $\Delta f = \Delta\rho c/2\pi(d_1 - d_0)$, if we have a room of size 6×6 meters, and the distance between Tx and Rx (d_0) is 4 meters, then the longest possible length of one-time-reflected path (d_1) is less than 15 meters, when Δρ is confined within $\pi/2$, the maximum allowable frequency difference is 6.8 MHz. If the WiFi card is configured with 40MHz bandwidth, then CSI values from adjacent OFDM subcarriers have bandwidth of 1.25MHz in Intel 5300 wireless NIC, according to 802.11n-2009 specification [8]. Therefore, we choose two CSI subcarriers that spacing every 5 indexes, i.e., 1 and 6, 2 and 7, etc.

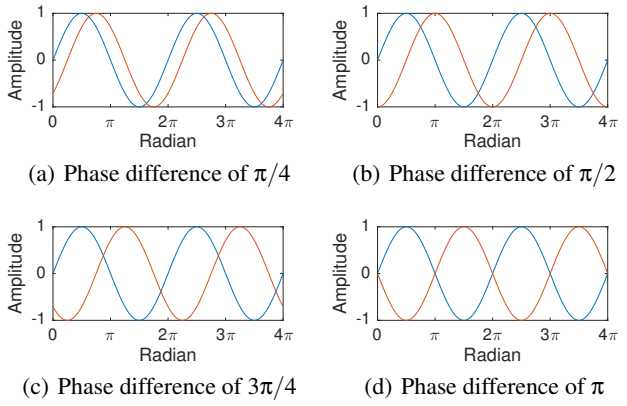

(a) Phase difference of $\pi/4$ (b) Phase difference of $\pi/2$

(c) Phase difference of $3\pi/4$ (d) Phase difference of π

Figure 5. Two waves with clear and ambiguous delay.

Phase Delay Estimation

Phase delay estimation between two CSI waveforms could be complicated. In signal processing, phase delay of two waveforms can be obtained by analytical methods. An analytical signal by Hilbert transformation of CSI waveform can give phase information and instantaneous frequency as function of time [21]. Precise phase extraction from analytical signal requires signal be mono-component, which means it contains only one frequency component at any given time. Chirp signal in radar is an example of such signal. Since perturbation of CSI waveforms caused by people moving is comprised of multiple frequency components[36], it's not easy to apply analytical method to extract phase delay directly.

However, time delay between two CSI waveforms conveys similar information as shown in Figure 3, and it can be measured in an easy way. Since torso of human body has much larger surface area than other parts such as arms and legs, it reflects much more signal and dominates fluctuations in CSI waveform while walking. By measuring the time delay of two subcarriers' waveforms, moving direction of human body can be inferred, and sign of this delay (positive or negative) is the direction information we want. Thus, we estimate the time delay between two CSI waveforms for direction estimation.

In signal processing, the most popular techniques for time delay estimation is generalized cross-correlation (GCC) method proposed by Knapp and Carter[13]. The process of correlation is useful in comparing two deterministic signals and it provides a measure of similarity between the first signal $x(t)$ and a time delayed version of the second signal $h(t+\tau)$ (or the first signal). Often times the second function $h(t)$ may be a corrupted version of $x(t)$, such as $h(t) = x(t) + n(t)$, where $n(t)$ is a noise signal [45]. In practice, we use cross-covariance to calculate delay. The covariance was defined as the correlation with the means subtracted out. Similarly, the cross-covariance was defined as the correlation left between two time series after subtracting out each means.

To be able to use cross-correlation to find the time delay, two signals must correlate, that is, they must look similar to certain extent. When a human is walking in the room, s/he does not change speed in a short timing window, say, 0.1 second. Therefore, we can treat the speed as constant in this period. The major design question is the choice of window size: if the window size is too small to cover a whole period, it cannot reliably estimate the mean value for delay estimation; if the window size is too large, people may walk in different speed during this window, and thus also lead to imprecise estimation. A normal person walks at speed from 0.3 to 2 m/s in indoor environments. In the Fresnel zone, the peak to peak distance is a bit larger than $\lambda/2$, which is about 3cm in WiFi 5GHz frequency band. Thus the CSI power fluctuates roughly (0.3, 2)/0.03 times per second, corresponding to 10 to 70 Hz. A 0.1 second window contains 1 to 7 periods. Therefore, we choose 0.1 second as the window size.

Fresnel Direction Estimation

So far we know the 0.1-second window is an appropriate parameter to estimate the time delay between the subcarriers, and thus the walking direction. In order to estimate the walking direction of a (sub) path, we need more data and compute statistics to make the result more robust. In reality, when walking, people don't change direction every second. Therefore, we use a 0.1 second sliding window with 50% overlay to measure delay within every 1 second time window. We aggregate positive and negative delay signs for each 1-second data as our statistic indicator of the Fresnel direction. For example, if a person has a positive Fresnel direction, then we have much more positive delays than negative ones, vice versa.

To validate and quantify the relationship between the moving direction and the estimated time delay, the Tx and Rx are placed 3 meters apart as shown in Figure 7, four straight line paths are chosen for small walking trials. Path 1 is almost parallel to tangent of ellipse, path 4 is perpendicular to tangent lines, and direction of path 2 and 3 are is evenly spaced between path 1 and 4. All the paths have the same length of 3 meters. Here we call *relative angle* as angle between walking path and LoS of Tx-Rx, then Path 1 have angle of 0 and Path 4 have angle of 90. The distribution of the delay estimations of path 1 and path 3 are shown in Figure 6.

We can see that when a person walks in path 3, it is easy to infer the walking direction - the majority of the delay values are positive and distributed at the right side to the zero point. For path 1, the delay values are approximately uniformly distributed around zero. By observing the delay distributions from this example, we are confident that our Fresnel direction estimation works when relative walking angle is greater than 30 degrees. Otherwise, we can't do Fresnel direction estimation based on the delay histogram. In reality, we need to empirically find a threshold to determine this angle.

In short, from the empirical study above, we learned that with only one Fresnel zone, we can not estimate the Fresnel direction for all the angles. In addition, the Fresnel direction is not equivalent to the direction in the real world (local Cartesian coordinate). As shown in Figure 7, both path 3 and 4 give outward information while their moving angles are totally different. It is natural to introduce another Fresnel zone to form a 2D Fresnel zone to address this issue.

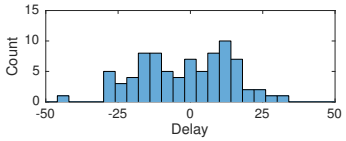

(a) Distribution of delay in Path 1

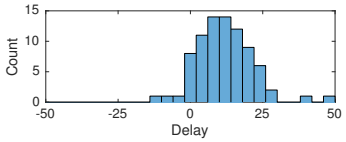

(b) Distribution of delay in Path 3

Figure 6. The delays are evenly distributed around zero in Path 1, while mostly seen in the postive side in Path 3.

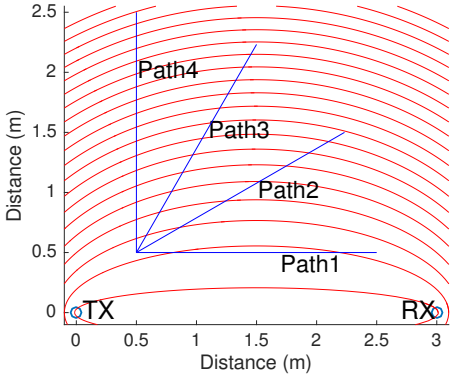

Figure 7. Experiment of walks for different angles for one pair of Tx-Rx. arcs are drawn every 3 ellipses for a clear view.

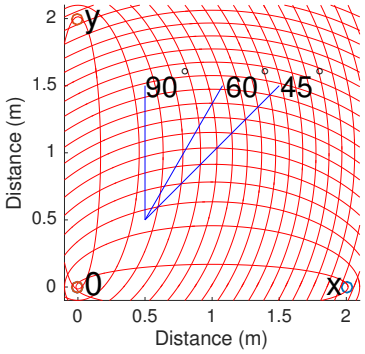

Figure 8. Placement of WiFi devices in a room and its Fresnel Zones. 3 directions to be test, arc lines are drawn every 3 ellipses for a clear view.

FROM FRESNEL DIRECTION TO LOCAL DIRECTION

To this end, we know what is Fresnel direction and how to estimate it using WiFi signals. In this section, we introduce two-dimensional (2D) Fresnel zones and how to estimate the walking direction in a local Cartesian coordinate system.

Direction and Distance Estimation in 2D Fresnel Zone

Recall that 1D Fresnel zone has significant limitations in estimating the walking direction. Intuitively, those problems can be mitigated if we have the same information from an orthogonal dimension. Let us assume we have a 2D Fresnel zone, as shown in Figure 8. We can clearly see that it immediately addresses the issue that we can't estimate the Fresnel direction when a reflector has a small relative angle in one Fresnel zone, because that means it is a large relative angle for another orthogonal Fresnel zone. In this way, we can estimate moving direction for all the moving angles in the target area.

To form this 2D Fresnel zone, we only need to bring another WiFi device. Let Tx be the origin of coordinate, Rx1 be direction of x axis and Rx2 be direction of y axis, we can see this 2D Fresnel zone creates an approximated local Cartesian coordinate system. Assume a human is moving from a to b, and our goal is to estimate the angle of $\overrightarrow{ab}$. So far we can estimate the sign of x and y components of $\overrightarrow{ab}$, and the next step is to estimate their magnitude (distance).

Distance in the Fresnel zone can be expressed as number of fluctuation periods. The method to count the number includes time domain approach (e.g. peaks counting, zero-cross counting, etc.) and frequency domain approach (FFT, rootMUSIC, etc.). We found peak counting and zero-cross counting are very sensitive to imperfect waveform thus are errors prone. So we choose frequency domain approach. To ensure real-time processing, we favor FFT over rootMUSIC. CSI wave-streams are sliced into windows and periods are counted one by one. The accuracy is listed as Table 1. The starting point is 0.5 meters away at perpendicular bisector of LoS, and Tx-Rx are separating 4 meters apart. We measure the ground-truth by using a laser range-finder, reference counts of fluctuations are calculated in Fresnel zone by measuring position of starting point and ending point. We can see that the errors are less than

Relative Angle (Degree)	Reference Fluctuations	Measured Fluctuations	Errors
90	72	69.5	-3.47%
60	66	65.1	-1.36%
45	60	62.6	4.33%
30	53	55	3.77%
15	45	53.2	18.22%

Table 1. Recorded fluctuation periods in 3 meters' paths, we see as relative moving angle goes smaller, the fluctuations measured exceed reference counts. the smaller walking direction the more accumulated error.

5% when relative direction angles are greater than 30 degrees, while jump to over 18% when angle is 15 degrees. Just the same as observation of direction estimation in the previous subsection, distance count estimation is not reliable at small angles.

We start from observations. In a room, two receivers are approximately symmetric about the line $y = x$, so we only examine 3 paths as shown in Figure 8. From the previous section we already know the Fresnel direction can be unreliable in certain cases. When a person starts to walk, s/he might go across multiple ellipses in both dimension in the 2D Fresnel zone. By taking the average of the estimated counts of the fluctuations from all subcarriers, we can infer the walking distance in each dimension. For example, for the path of relative angle of 60 degrees in Figure 8, we estimate that the person crossed 7.6 ellipses in y coordinate and 4.5 ellipses in x coordinate, and we have $\arctan(7.6/4.5) = 59.37$ degrees. In this case, the direction can be estimated by combining the Fresnel direction and distance estimation. Meanwhile, for the relative angle of 90 degrees, we have reliable information only from one dimension. Since fluctuation counts don't correspond to distance well in the other direction, we ignore distance and focus on delay distribution. Empirical study shows the more parallel to LoS, the more possible to accumulate a small absolute value for sign of delays in the whole path. In the same time, perpendicular side accumulates a large value of sign of delays. Combining this two information, we can give an approximate solution by taking accumulation of delay distribution as distance. It is not perfect but works for small angles most of

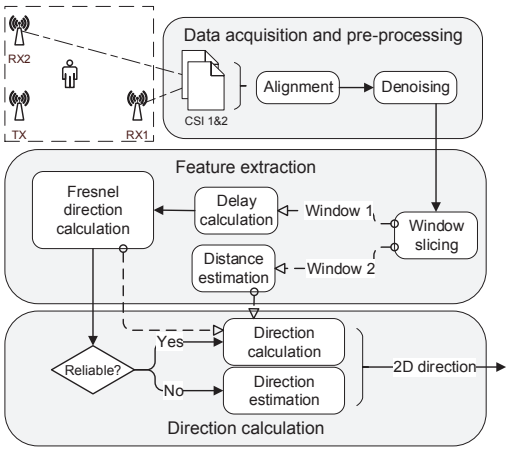

Figure 9. Information flow of WiDir. The inputs are two CSI data collected at Rx1 and Rx2, the output is 2D walking directions.

the time. For angles like 80 degrees, the method of summing up sign of delay still has a high probability to give the right Fresnel direction.

Local Direction in Cartesian Coordinate System

From above discussion, we have algorithm for two situations: if Fresnel directions are both reliable for two receivers, we have direction vector as $[sgn(dir_x)D_x, sgn(dir_y)D_y]^T$, where dir_x is the accumulated sign of delays in every 1-second time window and D_x is the distance in Fresnel model which measured as fluctuation counts, and sgn is the function given by $sgn(x) = -1, 0, 1$ for $x < 0, x = 0$ and $x > 0$, respectively. If one side of the two receivers has an unreliable Fresnel direction, we have direction vector as $[dir_x, dir_y]^T$.

EXPERIMENTAL EVALUATION

System Information Flow

Figure 9 shows the information flow of WiDir, which consists of three modules. Each module of WiDir represents one processing stage, namely: (1) data acquisition and pre-processing, (2) feature extraction and (3) direction estimation.

In data acquisition and pre-processing stage, CSI data are collected at Rx1 and Rx2 in the form of real-time streams and are sent to a computer to process. Firstly, two CSI wave-streams have to be aligned according to sync preambles broadcasted every few minutes. Then filtering techniques are applied to smooth out noisy signals.

In the second stage, two CSI wave-streams from Rx1 and Rx2 are processed separately. These data are sliced into small windows and keep sliding while processing. The features to be extracted include delay information and fluctuation counts within each window. Because the two feature extraction processes require different window sizes, CSI data are split into two steams. Delay is calculated between two subcarriers window by window, and the Fresnel direction is estimated by analyzing distribution of delays. Distance estimation is calculated by counting the number of fluctuations in frequency domain. The output of this stage is distance information and delay distribution for each pair of Tx-Rx over time.

The last stage is direction estimation. The algorithm is twofold depending on delay distributions. If both pair of Rxs have reliable Fresnel directions, then the direction is inferred by combining this information and distance information. While if one of the two Rxs has an unreliable Fresnel direction, then direction is estimated by an empirical method.

Implementation

WiDir consists of three components: A WiFi access point (AP) and two computers with wireless card. In our implementation, we use three Gigabyte BXi3H-5010 Brix mini-PCs with Intel 5300 wireless NIC installed, each equipped with external omni-directional antennas. Every miniPC has 2G memory and runs Ubuntu 14.04 LTS. An additional computer is used to process CSI data in real-time using MATLAB. CSI data were collected at two receivers using tools developed by Halperin *et al* [4], then passed to processing computer via TCP/IP protocol. The transmitter is configured to send packets in injection mode. Transmitter drops some packets every 10 seconds in a predefined pattern to act as a sync signal. Two receivers can therefore align data with each other according to this signal.

The experiment in this paper was performed at 5GHz frequency band with 40MHz bandwidth. 5GHz band has shorter wavelength than 2.4GHz band which produce twice the number of fluctuations, the phase delay from two subcarriers is clearer when walking a short distance.

Typical walking speed indoors is from 0.3 to 2 meters per second, which means the fluctuation is roughly 10 to 70Hz in 5GHz frequency band according to Fresnel model. Our sampling rate is set to 500 packets per second, which is fast enough to capture this information.

Data Denoising

CSI data collected at commercial WiFi device is very noisy. In the traditional signal cross-correlation process, two signals can be compared for delay directly without denoising, provided these two signals come from exactly the same copy. In WiDir, cross-correlation is used to measure signal similarities between two OFDM subcarriers. This process is noise sensitive, so denoising is a non-trivial step. By using cross-correlation to compare subcarriers, we need data from all the subcarriers and keep their phase unaltered after filtering. In this case, dimensionality reduction based method (e.g. PCA) and FIR based filtering solution is not appropriate here. At the same time, the fluctuation pattern caused by people walking may contain low frequency and high frequency components simultaneously, a IIR low-pass filter cannot efficiently smooth out signal while maintain shape of the waveform.

To solve this problem, we use Savitzky-Golay filter to smooth signal. Savitzky-Golay filter (also called digital smoothing polynomial filters or least-squares smoothing filters) fits successive subset of data points with low degree polynomial by the method of linear least square [30]. It can smooth signal without greatly distort it as shown in Figure 10. Note that it is important to keep shape and thus preserve phase information in signals.

WiDir is computationally efficient and capable to run in real-time. In a laptop with i7-2620 CPU and 4GB memory, WiDir

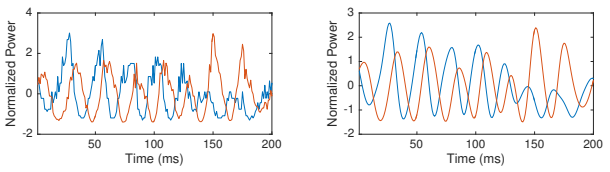

(a) Raw CSI waveform (b) Denoised CSI waveform

Figure 10. Raw CSI waveform and denoised waveform using Savitzky-Golay smoothing.

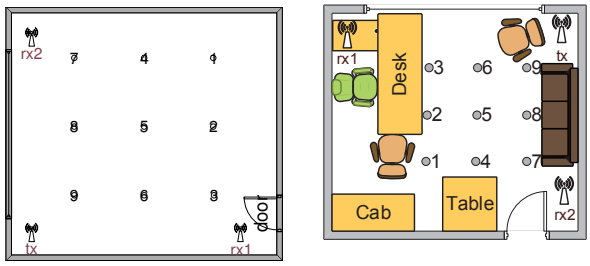

(a) Room A: an empty room (b) Room C: an office room

Figure 11. Experiment settings in Room A and Room C. There are nine locations in the room, namely 1-9. Directions are measured between these points.

uses 35ms to process 1 second CSI data at sampling rate of 500 in MATLAB. It is possible to further improve performance by leveraging general purpose GPU accelerations such as nVidia CUDA.

Experimental Setup

WiFi transmitter and receivers are placed in the three corners of the rooms as shown in Figure 11. All three equipments are mounted on tripods and the antennas' height is 1.5 meters above ground. The coordinates of each device are marked by a Bosch GLM-80 laser range-finder. Totally 1289 paths from 5 volunteers are collected, each path is a predefined straight line of approximately 2 meters. Coordinates of start point and end point of the paths are measured by laser range-finder and are converted into moving angles for reference. Directions are estimated every second. If people take more than one second to walk along the path, average angle of the whole path is used. The threshold of delay distribution to distinguish reliable and unreliable Fresnel direction is set at one quarter of the window.

Evaluation

We perform the experimental evaluation in three rooms. Room A is an empty room of size 6×7m. Room B is a student activity room of size 6×6m. There are five tables and twenty chairs in room B, one of the tables is a big metal table sized 1.5×4m. The tables and chairs are rearranged before the test to make room for walking. Room C is a normal office room of size 4×3m. It has two desks, a sofa, a cabinet and three chairs.

Accuracy of Eight Basic Directions

We first present the accuracy WiDir achieves in detecting four groups of paths' direction in three rooms. Each group contains 3 paths which are in parallel and of the same length.

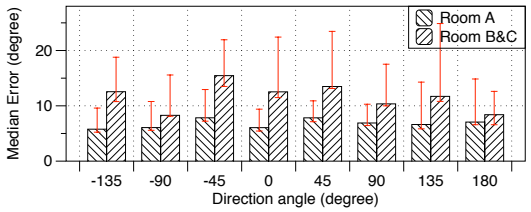

(a) Median absolute error of empty room and office rooms

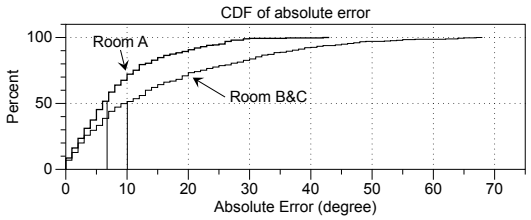

(b) CDF of absolute error for empty room and office rooms

Figure 12. Result of eight basic directions in empty room (A) and office rooms (Room B and C)

Volunteers walk along these paths back and forth, so each path has two directions. The four groups covered eight basic directions each separated 45 degrees apart. Because there are tables and cabinets in the rooms, the actual walking space is limited in the center of the room. We use an empty Room A as a base line to compare with other two multi-path rich rooms, Figure 11 shows the experiment settings in Room A and Room C. The settings in Room B are similar except that the furniture is different.

We collect 856 paths in room A, and 433 paths in room B and room C. The results are shown in median absolute error. We also calculated 95% confidence interval using bootstrap method. Results of Room A, B and C are compared in Figure 12(a) in bar graph with 95% confidence interval.

The overall Mean Absolute Error in the empty room (Room A) is 10.538 degrees, and deviation is 8.174. And overall Mean Absolute Error in room B and room C is 15.510 degrees, and deviation is 13.964. Cumulative Distribution Function (CDF) of absolute error for all the directions in Room A and Room B&C are compared in Figure 12(b). The evaluation results show that the overall absolute median error in a normal room is 11.102 degrees. And the overall absolute median error in an empty room is 8.623 degrees.

Sensitivity of Different Angles

In this section, we choose some paths other than eight basic directions. We choose two start points in Room B, each has 5 paths in different directions. Path name like (9 → 3) means walk from location 9 to location 3, as shown in Figure 11(a). We have 2 volunteers to walk through these paths, each path walks eight times. Direction of each path is an average of all the measured angles for this path. Reference directions and measured directions are listed in Table 2. We can see in a multi-path rich room (Room B), walking directions other than the eight basic directions have comparable results. Mean absolute error is about 10 degrees except path (6 → 8). By examining room environment we found a metal table is in

Path	Reference Angle	Mean Absolute Error	Median Absolute Error	Standard Deviation
$9 \rightarrow 3$	0	7.318	7.318	7.450
$9 \rightarrow 2$	26.565	8.498	7.318	9.413
$9 \rightarrow 1$	45	9.738	8.253	8.342
$9 \rightarrow 4$	63.435	11.848	10.330	6.607
$9 \rightarrow 7$	90	10.254	8.297	6.532
$6 \rightarrow 2$	45	7.259	5.401	7.024
$6 \rightarrow 1$	63.435	7.792	9.091	3.865
$6 \rightarrow 4$	90	6.824	6.401	4.820
$6 \rightarrow 7$	116.565	10.191	10.062	6.312
$6 \rightarrow 8$	135	16.319	12.844	12.753

Table 2. Reference angles and measured angles for different paths. Unit is in degree.

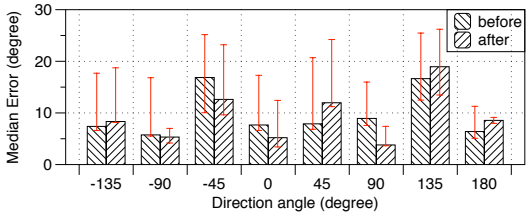

(a) Median absolute error before and after move furnitures

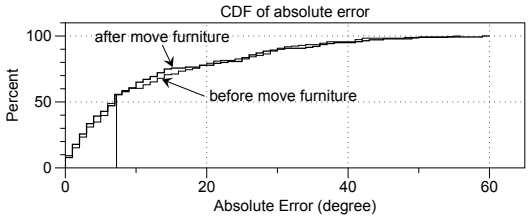

(b) CDF of absolute error before and after move furnitures

Figure 13. Result of eight basic directions before and after environmental changes in an office room (Room C).

opposite to path ($6 \rightarrow 8$), the result angle influenced greatly by reflection of the metal in the middle point of this path. However, this strong metal reflection doesn't have the same magnitude of impact on other paths.

Resilience of environment change

In this part we carried out a two-step experiment in a small office room (Room C) to detect eight basic directions. The settings in the first step are illustrated in Figure 11(b). Then before the second step, we moved the sofa by 1 meter and moved two armchairs to another side of the room to simulate environmental changes. Each path is walked four times by two volunteers. The errors are compared for the two situations.

The results of eight basic directions before and after furniture move are shown in Figure 13. The overall mean absolute error before and after furniture move are 12.291 and 12.120 degrees, and median absolute error are 7.480 and 7.242 degrees, respectively. We can see that environmental change have insignificant impact on the result.

Continuous Walking Show

In the previous subsections, we presented the evaluation results of the walks following straight lines. Here we show WiDir can measure continuously changed directions. The two tracks we

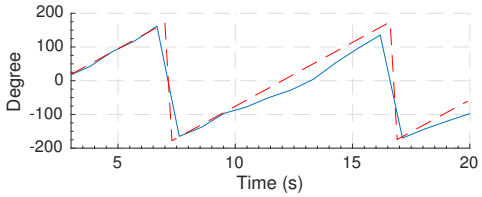

(a) Directions when follow a circle

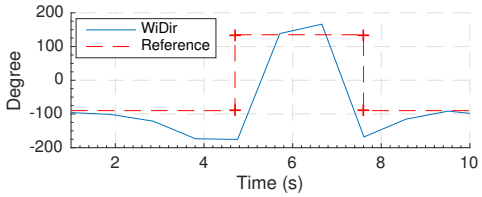

(b) Directions when follow a zigzag

Figure 14. Continuous walking of circle and zigzag.

chose to walk are circle and zigzag. For the path with the circle pattern, we drew a circle in the middle of the room, and divided the circle into equal pieces and marked it before we walk. Volunteers are required to keep constant slow speed to move from one mark to another according to beats of a metronome. Starting position in the circle is chosen and moving direction is towards zero degree. The reference angles are calculated based on total walking time of a whole circle. The zigzag path is defined by walking through 4 locations one by one (1-3-7-9) in straight lines. Reference angles are decided by dividing the whole walking time into three segments according to video recordings. The results are shown in Figure 14, reference directions are in red dashed lines.

The results are pretty well when walking a circle, but not that good when following zigzag. In the middle of each segment of zigzag, the result matches reference angle, but at every turning point of zigzag the errors going larger.

LIMITATIONS AND DISCUSSION

Multi-path Influence

Multi-path is known to be the major error source for RF-based human centric sensing applications, such as localization, gesture recognition. WiDir is no exception. The main reasons are that a) human as a reflector will induce extra multi-path than the major one we assume in our model. b) When a human subject is walking in the room, (s)he will block environmental static paths and thus distorts Fresnel zone shape. Particularly, we observe the angular error can be as large as 40 degrees when a metal is nearby. We can potentially address this issue as long as the metal is in vicinity of only small part of the path based on backward analysis.

Grid Approximation

We use the intersected equiphase contours from two Fresnel zones to approximate the grid for distance estimation, which lead to three potential issues. First, the contour does not have the same slope as straight line. It is required to perform a mathematical transformation to perform the right-angle processing. Second, in a Fresnel zone, the space between adjacent

equiphase contours will decrease as the phase increases, which means the size of the squares in the grid are not the same. Third, most rooms are not square, and thus their corresponding Fresnel zones are of different shape and size. All these factors will contribute to the errors in distance estimation in certain region of the target area. However, if it is possible to estimate Fresnel phase of the signal in commodity WiFi device, we can estimate the human location by calculating distance to WiFi device pairs from phase delays and further address the issue in our future work.

Detection Range and Device Placement

Radio signals get attenuated as they propagate. As people walk further away relative to the center of Fresnel zones, they cause smaller impact on the received signal strength. Therefore, the detection range is limited if only one pair of WiFi devices is used. To extend the detection area (hopefully full coverage), especially for a large space such as conference room and hallway, it is natural to address this problem by deploying more WiFi devices since they can form more Fresnel zones. It is important to design an algorithm to combine multiple (dis)joint local Fresnel zones into a global one to facilitate walking direction estimation. Meanwhile, the number of devices increases at the cost of introducing more interference. Therefore, it is important to minimize the number of WiFi devices while still achieving the desirable detection accuracy, which leads to an optimal device placement problem for our future work.

Multiple People

WiDir focuses on personal sensing and our solution works for one person in typical indoor environments. A natural question will be: can and how WiDir scale to more people? When multiple people co-exist in the target area, they will cause additive effect at the receiver side, which could be sequentially estimated based on the rationale of successive cancellation, as studied in [44, 2] for other device-free sensing applications. For example, people can cause changes on the received signal strength of different Tx-Rx pairs [44]. It is also observed in [2] that reflections off the nearest person can have much more power than distant reflections. WiDir can leverage multiple pairs of Tx-Rx and employ similar approaches to work for the scenario of multiple people. However, successive cancellation based techniques can only work well when people are not close to each other, as illustrated in [44]. In addition, CSI data collected from COTS WiFi NICs are mixed with rich hardware distortions in both power strength [36] and phase [43]. It is still very challenging to fully address this problem.

RELATED WORK

There are many existing work presenting different techniques of WiFi-based device-free sensing and device-based walking direction estimation, which is clearly different from our work.

Device-based Human Walking direction: In this type of work, most techniques rely on inertial sensors more or less. Foot is one of the best place to put on-body sensors to analyze the walking direction. The work presented in [12] leverages gyroscope and magnetic compass data to estimate the walking direction. In [39], the authors combine the inertial unit, a detailed building model, and a particle filter to provide the walking direction the indoor location. Another thread is smartphone-based approach with different user-centric assumption. For example, the work presented in [16] infer orientation by identifying human gesture like texting. In [18], the authors assume that the initial orientation of the phone is known. WalkCompass [28] removes the magnetic interference in indoor environments to improve the results.

WiFi-based Device-free Sensing: This set of techniques can be traced back as early as 2007. At that time, most techniques were using received signal strength indicator (RSSI). The authors in [46] proposed a fingerprinting based approach for indoor localization while the work presented in [47] took a geometric approach to detect the human motion. RTI [38] was proposed to use tomographic reconstruction to estimate an image of human presence. Later, CSI was recognized as a better radio signal source to cope with multipath since it provides finer grained information. Fall was detected use CSI in [6, 48, 34]. Zhou et al. proposed to use CSI to detect human presence in an environment [49]. Xi et al. proposed to use CSI to count the number of people for crowd estimation [41]. WiHear uses specialized directional antennas to obtain CSI variations caused by lip movement for recognizing spoken words [33] [26]. E-eyes [37] recognizes a set of nine home human activities using CSI. C^2IL estimate the moving speed and distance using ripples in CSI power [9], CARM relates signal fluctuations to total length of paths and number of fluctuations to moving distance using CSI-speed model [36] .

CONCLUSION

This paper demonstrates that human walking direction can be estimated using off-the-shelf WiFi devices already everywhere in our daily life, without requiring users to carry any device. The core techniques are rooted in the theory of Fresnel zone based multi-frequency phase analysis introduced in this work. We further apply this theory and extend to multi-dimensional Fresnel zone space which can be naturally formed by multiple pairs of WiFi devices in today's typical indoor environments to improve scalability. We conduct comprehensive theoretical studies and our experimental results show that WiDir can estimate human walking direction with overall median absolute angle error less than 10 degrees in different indoor environments. The obtained results not only justify the theory we developed, but also provide basic principles and practical guidelines for building cost-effective WiFi CSI-based human walking direction estimation systems. We believe not only this new context can immediately help many context-aware applications, such as localization, augmented reality and assisted living, the theory also can be applied in a wider range of macro/micro human activity recognition based applications.

ACKNOWLEDGMENTS

We would like to thank Yuxiang Wang and Ruiyang Gao for their help during the experiments. This research is supported by National Key Research and Development Plan under Grant No.2016YFB1001200, NSFC Grant No. 61572048, and Peking University Key Discipline Construction Grant.

REFERENCES

1. Heba Abdel-Nasser, Reham Samir, Ibrahim Sabek, and Moustafa Youssef. 2013. MonoPHY: Mono-stream-based device-free WLAN localization via physical layer information. In *Proc. of WCNC*. IEEE.
2. Fadel Adib, Zachary Kabelac, and Dina Katabi. 2015. Multi-person localization via rf body reflections. In *Proc. of NSDI*. USENIX.
3. Yongtae Do and Jongman Kim. 2013. Infrared range sensor array for 3D sensing in robotic applications. *International Journal of Advanced Robotic Systems* 10 (2013).
4. Daniel Halperin, Wenjun Hu, Anmol Sheth, and David Wetherall. 2011. Tool release: gathering 802.11 n traces with channel state information. *ACM SIGCOMM Computer Communication Review* 41, 1 (2011), 53–53.
5. JM Hamilton, BS Joyce, ME Kasarda, and PA Tarazaga. 2014. Characterization of human motion through floor vibration. In *Dynamics of Civil Structures, Volume 4*. Springer, 163–170.
6. Chunmei Han, Kaishun Wu, Yuxi Wang, and Lionel M Ni. 2014. WiFall: Device-free fall detection by wireless networks. In *Proc. of INFOCOM*. IEEE.
7. Hristo D Hristov. 2000. *Fresnal Zones in Wireless Links, Zone Plate Lenses and Antennas*. Artech House, Inc.
8. IEEE. 2009. IEEE Standard for Information technology–Local and metropolitan area networks– Specific requirements– Part 11: Wireless LAN Medium Access Control (MAC)and Physical Layer (PHY) Specifications Amendment 5: Enhancements for Higher Throughput. *IEEE Std 802.11n-2009* (2009), 1–565.
9. Zhi-Ping Jiang, Wei Xi, Xiangyang Li, Shaojie Tang, Ji-Zhong Zhao, Jin-Song Han, Kun Zhao, Zhi Wang, and Bo Xiao. 2014. Communicating is crowdsourcing: Wi-Fi indoor localization with CSI-based speed estimation. *Journal of Computer Science and Technology* 29, 4 (2014), 589–604.
10. Ming Jin, Han Zou, Kevin Weekly, Ruoxi Jia, Alexandre M Bayen, and Costas J Spanos. 2014. Environmental sensing by wearable device for indoor activity and location estimation. In *Proc. of IECON*. IEEE.
11. Ossi Kaltiokallio, Huseyin Yigitler, Riku Jantti, and Neal Patwari. 2014. Non-invasive respiration rate monitoring using a single COTS TX-RX pair. In *Proc. of IPSN*. IEEE.
12. Jeong Won Kim, Han Jin Jang, Dong-Hwan Hwang, and Chansik Park. 2004. A step, stride and heading determination for the pedestrian navigation system. *Positioning* 1, 08 (2004), 0.
13. Charles Knapp and Glifford Carter. 1976. The generalized correlation method for estimation of time delay. *IEEE Transactions on Acoustics, Speech, and Signal Processing* 24, 4 (1976), 320–327.
14. Ahmed E Kosba, Ahmed Saeed, and Moustafa Youssef. 2012. Rasid: A robust wlan device-free passive motion detection system. In *Proc. of PerCom*. IEEE.
15. Manikanta Kotaru, Kiran Joshi, Dinesh Bharadia, and Sachin Katti. 2015. SpotFi: Decimeter Level Localization Using WiFi. In *Proc. of SIGCOMM*. ACM.
16. Fan Li, Chunshui Zhao, Guanzhong Ding, Jian Gong, Chenxing Liu, and Feng Zhao. 2012. A reliable and accurate indoor localization method using phone inertial sensors. In *Proc. of UbiComp*. ACM.
17. Qinghua Li and Guohong Cao. 2013. Providing privacy-aware incentives for mobile sensing. In *Proc. of PerCom*. IEEE.
18. Jó Ágila Bitsch Link, Paul Smith, Nicolai Viol, and Klaus Wehrle. 2011. FootPath: Accurate map-based indoor navigation using smartphones. In *Proc. of IPIN*. Citeseer.
19. Jian Liu, Yan Wang, Yingying Chen, Jie Yang, Xu Chen, and Jerry Cheng. 2015. Tracking Vital Signs During Sleep Leveraging Off-the-shelf WiFi. In *Proc. of MobiHoc*. ACM.
20. Xuefeng Liu, Jiannong Cao, Shaojie Tang, and Jiaqi Wen. 2014. Wi-Sleep: Contactless sleep monitoring via WiFi signals. In *Proc. of RTSS*. IEEE.
21. Lawrence Marple. 1999. Computing the discrete-time "analytic" signal via FFT. *IEEE Transactions on signal processing* 47, 9 (1999), 2600–2603.
22. Pedro Melgarejo, Xinyu Zhang, Parameswaran Ramanathan, and David Chu. 2014. Leveraging directional antenna capabilities for fine-grained gesture recognition. In *Proc. of UbiComp*. ACM.
23. Neal Patwari, Lara Brewer, Quinn Tate, Ossi Kaltiokallio, and Maurizio Bocca. 2014. Breathfinding: A wireless network that monitors and locates breathing in a home. *IEEE Journal of Selected Topics in Signal Processing* 8, 1 (2014), 30–42.
24. Qifan Pu, Sidhant Gupta, Shyamnath Gollakota, and Shwetak Patel. 2013. Whole-home gesture recognition using wireless signals. In *Proc. of MobiCom*. ACM.
25. Kun Qian, Chenshu Wu, Zheng Yang, Yunhao Liu, and Zimu Zhou. 2014. PADS: passive detection of moving targets with dynamic speed using PHY layer information. In *Proc. of ICPADS*. IEEE.
26. Theodore Rappaport. 2001. Wireless Communications: Principles and Practice. (2001).
27. Ruth Ravichandran, Elliot Saba, Ke-Yu Chen, Mayank Goel, Sidhant Gupta, and Shwetak N Patel. 2015. WiBreathe: Estimating respiration rate using wireless signals in natural settings in the home. In *Proc. of PerCom*. IEEE.
28. Nirupam Roy, He Wang, and Romit Roy Choudhury. 2014. I am a smartphone and i can tell my user's walking direction. In *Proc. of MobiSys*. ACM.

29. Stefano Savazzi, Stephan Sigg, Monica Nicoli, Vittorio Rampa, Sanaz Kianoush, and Umberto Spagnolini. 2016. Device-Free Radio Vision for Assisted Living: Leveraging wireless channel quality information for human sensing. *IEEE Signal Processing Magazine* 33, 2 (2016), 45–58.
30. Ronald W Schafer. 2011. What is a Savitzky-Golay filter?[lecture notes]. *Signal Processing Magazine, IEEE* 28, 4 (2011), 111–117.
31. Björn Schuller, Florian Pokorny, Stefan Ladstätter, Maria Fellner, Franz Graf, and Lucas Paletta. 2013. Acoustic geo-sensing: Recognising cyclists' route, route direction, and route progress from cell-phone audio. In *Proc. of ICASSP*. IEEE.
32. Ching-Sheng Wang and Chien-Liang Chen. 2014. RFID-based and Kinect-based indoor positioning system. In *Proc. of VITAE*. IEEE.
33. Guanhua Wang, Yongpan Zou, Zimu Zhou, Kaishun Wu, and Lionel M Ni. 2014. We can hear you with wi-fi!. In *Proc. of MobiCom*. ACM.
34. Hao Wang, Daqing Zhang, Yasha Wang, Junyi Ma, Yuxiang Wang, and Shengjie Li. 2016. RT-Fall: A Real-time and Contactless Fall Detection System with Commodity WiFi Devices. *IEEE Transactions on Mobile Computing* (2016), 1–1.
35. Sheng Shih Wang, Kuei Ping Shih, and Chih Yung Chang. 2007. Distributed direction-based localization in wireless sensor networks. *Computer Communications* 30, 6 (2007), 1424–1439.
36. Wei Wang, Alex X Liu, Muhammad Shahzad, Kang Ling, and Sanglu Lu. 2015. Understanding and modeling of wifi signal based human activity recognition. In *Proc. of MobiCom*. ACM.
37. Yan Wang, Jian Liu, Yingying Chen, Marco Gruteser, Jie Yang, and Hongbo Liu. 2014. E-eyes: device-free location-oriented activity identification using fine-grained wifi signatures. In *Proc. of MobiCom*. ACM.
38. Joey Wilson and Neal Patwari. 2010. Radio tomographic imaging with wireless networks. *IEEE Transactions on Mobile Computing* 9, 5 (2010), 621–632.
39. Oliver Woodman and Robert Harle. 2008. Pedestrian localisation for indoor environments. In *Proc. of UbiComp*. ACM.
40. Kaishun Wu, Jiang Xiao, Youwen Yi, Dihu Chen, Xiaonan Luo, and Lionel M Ni. 2013. CSI-based indoor localization. *IEEE Transactions on Parallel and Distributed Systems* 24, 7 (2013), 1300–1309.
41. Wei Xi, Jizhong Zhao, Xiang-Yang Li, Kun Zhao, Shaojie Tang, Xue Liu, and Zhiping Jiang. 2014. Electronic frog eye: Counting crowd using wifi. In *Proc. of INFOCOM*. IEEE.
42. Jiang Xiao, Kaishun Wu, Youwen Yi, Lu Wang, and Lionel M. Ni. 2013. Pilot: Passive Device-Free Indoor Localization Using Channel State Information. In *Proc. of ICDCS*. IEEE.
43. Yaxiong Xie, Zhenjiang Li, and Mo Li. 2015. Precise Power Delay Profiling with Commodity WiFi. In *Proc. of MobiCom*. ACM.
44. Chenren Xu, Bernhard Firner, Robert S Moore, Yanyong Zhang, Wade Trappe, Richard Howard, Feixiong Zhang, and Ning An. 2013. Scpl: indoor device-free multi-subject counting and localization using radio signal strength. In *Proc. of IPSN*. IEEE.
45. R.K. Rao Yarlagadda. 2010. *Analog and digital signals and systems*. Vol. 1. Springer.
46. Moustafa Youssef, Matthew Mah, and Ashok Agrawala. 2007. Challenges: device-free passive localization for wireless environments. In *Proc. of MobiCom*. ACM.
47. Dian Zhang, Jian Ma, Quanbin Chen, and Lionel M Ni. 2007. An RF-based system for tracking transceiver-free objects. In *Proc. of PerCom*. IEEE.
48. Daqing Zhang, Hao Wang, Yasha Wang, and Junyi Ma. 2015. Anti-fall: A non-intrusive and real-time fall detector leveraging CSI from commodity WiFi devices. In *Proc. of ICOST*. Springer.
49. Zimu Zhou, Zheng Yang, Chenshu Wu, Longfei Shangguan, and Yunhao Liu. 2013. Towards omnidirectional passive human detection. In *Proc. of INFOCOM*. IEEE.